Unidirectional spin transport of a spin-orbit-coupled atomic matter wave using a moving Dirac δ-potential well

Jieli Qin[1,*] and Lu Zhou[2,3,†]

[1]*School of Physics and Electronic Engineering, Guangzhou University, 230 Wai Huan Xi Road, People's Republic of China and Guangzhou Higher Education Mega Center, Guangzhou 510006, People's Republic of China*

[2]*Department of Physics, School of Physics and Electronic Science, East China Normal University, Shanghai 200241, People's Republic of China*

[3]*Collaborative Innovation Center of Extreme Optics, Shanxi University, Taiyuan, Shanxi 030006, People's Republic of China*

(Received 13 April 2020; accepted 16 June 2020; published 6 July 2020)

We study the transport of a spin-orbit-coupled atomic matter wave using a moving Dirac δ-potential well. In a spin-orbit-coupled system, bound states can be formed in both ground and excited energy levels with a Dirac δ potential. Because Galilean invariance is broken in a spin-orbit-coupled system, moving of the potential will induce a velocity-dependent effective detuning. This induced detuning breaks the spin symmetry and makes the ground-state transporting channel be spin-$\uparrow$ ($\downarrow$) favored while makes the excited-state transporting channel be spin-$\downarrow$ ($\uparrow$) favored for a positive-direction (negative-direction) transporting. When the δ-potential well moves at a small velocity, both the ground-state and the excited-state channels contribute to the transportation, and thus both the spin components can be efficiently transported. However, when the moving velocity of the δ-potential well exceeds a critical value, the induced detuning is large enough to eliminate the excited bound state, and makes the ground bound state the only transporting channel, in which only the spin-$\uparrow$ ($\downarrow$) component can be efficiently transported in a positive (negative) direction. This work demonstrates a prototype of unidirectional spin transport.

DOI: 10.1103/PhysRevA.102.013304

I. INTRODUCTION

Transport of matter waves is essential in many ultracold-atom physics experiments and applications. With such a technique, an ultracold-atom experiment can be split into matter-wave-producing and matter-wave-using modules. Each module can be optimized separately. Thus the experiment can be performed more efficiently [1–3]. In this vein of thought, for example, atomic gases have been loaded into optical cavities [4–9] and hollow fibers [10–14], leading to a good many interesting research works (for reviews, see Refs. [15–17]). It is also found that the transport of atomic matter waves can be very useful in the realization of atom interferometry [18–20], atomtronics devices [21–24], and continuous atom lasers [25–27].

Many schemes to transport cold atomic matter waves have been demonstrated. In the moving molasses technique [28,29], the cloud of cold atoms freely flies to the destination by itself. Controlled transport can be realized by applying an atomic waveguide [30–40]. However, using these techniques, the cloud of atoms expands, and its density drops during the transporting process. To overcome this blemish, the transport of matter waves using a moving potential well is introduced and soon becomes widely used in cold-atom experiments [1–3,26,41–46].

The moving dynamic of spin-orbit (SO)-coupled matter waves shows new features. For a SO-coupled system, the Galilean invariance does not hold any more [47–49]. Different moving directions or speeds can have very different effects on the dynamics of SO-coupled atomic gases. As a result, many interesting phenomena arise. A few examples are listed below. The critical velocity of superfluidity becomes reference frame dependent [50]. An oscillation of magnetization in SO-coupled Bose-Einstein condensate (BEC) is induced by the moving [51,52]. The shape of a SO-coupled BEC bright soliton changes with its velocity [53] . In a translating optical lattice, a SO-coupled BEC behaves anisotropically depending on the direction of translation [54]. The normal density of superfluidity does not vanish even at zero temperature [55]. And, nonmagnetic one-way spin switch [56] and spin-current generation [57] have also been demonstrated recently.

In this paper, we study the transport of a SO-coupled cold atomic matter wave using a moving Dirac δ-potential well (see Fig. 1). We show that the δ-potential well can at most support both a ground state and an excited bound state in a SO-coupled cold-atom system. These bound states can be used to efficiently transport the cold atomic matter wave and thus serve as the transporting channels in the problem. Moving of the potential well will induce a velocity-proportional effective detuning, which can substantially affect the transporting channels. This induced detuning breaks the spin symmetry and makes the two transporting channels spin-polarized. For a slow positive-direction moving δ-potential well, the ground-state channel is spin-$\uparrow$ favored, while the excited-state channel

*104531@gzhu.edu.cn; qinjieli@126.com
†lzhou@phy.ecnu.edu.cn

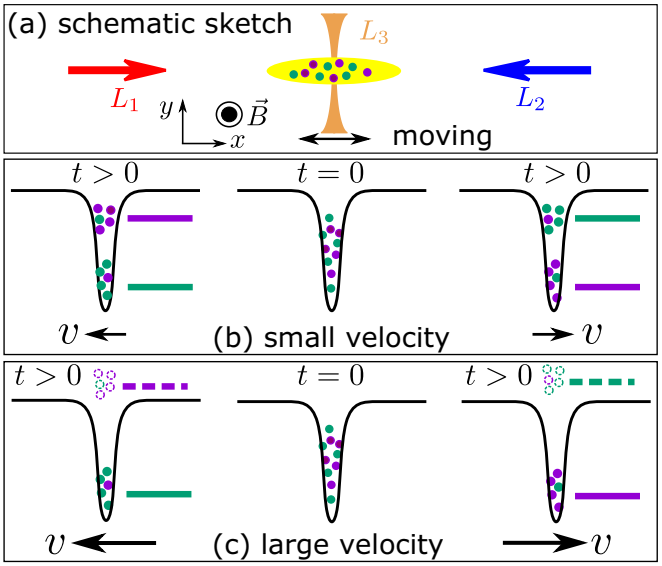

FIG. 1. Diagram of the transport of a SO-coupled cold atomic matter wave using a moving δ-potential well. At time $t = 0$, an atomic SO-coupled BEC is prepared in the ground state of a δ-potential well. The atoms are equally distributed in the spin-$\uparrow$ and spin-$\downarrow$ components. Afterward, one moves the δ-potential well at velocity v to transport the matter wave. (a) Schematic sketch of the system. The SO coupling is realized by the two counterpropagating Raman lasers L_1 and L_2. The third tightly focused movable laser beam, L_3, generates the δ-potential well. (b) For a small-velocity moving δ-potential well, it can support two transporting channels—ground and excited bound states of the moving δ-potential well in the comoving frame. One of the transporting channels is spin-$\uparrow$ favored, while the other one is spin-$\downarrow$ favored. Both the spin-$\uparrow$ and the spin-$\downarrow$ components can be efficiently transported in such a case. (c) For a large-velocity moving δ-potential well, the moving-induced effective detuning lifts the excited state out of the binding ability of the potential well; thus matter-wave transportation can only take place in the ground-state channel. For a positive-direction (negative-direction) moving δ-potential well, the ground-state channel is spin-$\uparrow$ (spin-$\downarrow$) dominant, thus only the spin-$\uparrow$ (spin-$\downarrow$) component can be efficiently transported.

is spin-$\downarrow$ favored. Both the spin-$\uparrow$ and the spin-$\downarrow$ components can be transported through their favorable channel. For a slow negative-direction moving δ-potential well, things are very similar, except that the roles of spin-$\uparrow$ and spin-$\downarrow$ exchange with each other. When the velocity of the moving δ-potential well exceeds a critical value, the induced effective detuning will be large enough to lift the excited state out of the binding ability of the δ-potential well, thus eliminating the excited bound-state transporting channel. Therefore, in such a case, a matter wave can only be transported through the ground-state channel. Since for a positive-direction (negative-direction) moving δ-potential well, the ground-state channel is spin-$\uparrow$ (spin-$\downarrow$) dominant, only this appropriate spin component of the matter wave can be efficiently transported. These unidirectional transporting features indicate that the system considered here may potentially be used to realize spintronic devices such as spin diodes [58,59], valves [60], and filters [61,62].

This paper is organized as follows: In Sec. II, the physical model of this paper is presented. In Sec. III, we solve the bound states (i.e., the transporting channels) of the moving δ-potential well and discuss their properties. In Sec. IV, the transporting dynamics and efficiency are shown. At last, the paper is summarized in Sec. V.

II. MODEL

We consider the transporting of quasi-one-dimensional SO-coupled cold atoms using a moving δ-potential well (see Fig. 1). The SO coupling is realized by the two x-direction counterpropagating Raman lasers L_1 and L_2 [63]. And the δ-potential well can be generated using a y-direction-shining tightly focused laser beam [64,65]. Such a system can be described by the Hamiltonian

$$H = H_0 + U(x,t), \tag{1}$$

where $U(x,t)$ is the external potential, and H_0 is the SO-coupled free-particle Hamiltonian:

$$H_0 = \begin{bmatrix} \frac{(p_x-p_c)^2}{2m} - \frac{\hbar\Delta_0}{2} & \frac{\hbar\Omega}{2} \\ \frac{\hbar\Omega}{2} & \frac{(p_x+p_c)^2}{2m} + \frac{\hbar\Delta_0}{2} \end{bmatrix}. \tag{2}$$

Here $p_x = \hbar k_x = -i\hbar\frac{\partial}{\partial x}$ is the one-dimensional momentum operator, $p_c = \hbar k_c$ is the strength of the SO coupling determined by momentum transfer during the Raman scattering process, Δ_0 is the detuning of the Raman driving from the atomic energy level splitting (in this paper we assume that its value is set to zero, $\Delta_0 = 0$), and Ω is the effective Rabi frequency for Raman flipping between the two spin states. The interatom collision interaction is not included here, as it is assumed to have been eliminated by the Feshbach resonance technique [66,67]. In the following, for convenience the natural unit $\hbar = m = 1$ is used.

Before time $t = 0$, the system is prepared in the ground state of a δ-potential well localized at $x = 0$. Then, for time $t > 0$, we move the δ-potential well at a constant velocity, v, and study the subsequent transportation. Hence, the external potential $U(x,t)$ can be written in a piecewise function as follows:

$$U(x,t) = \begin{cases} V_0(x) = -V_0\delta(x), & t \leqslant 0, \\ V(x,t) = -V_0\delta(x - vt), & t > 0. \end{cases} \tag{3}$$

The initial state can be constructed using the free-particle oscillating evanescent wave modes (for detail, see Sec. III):

$$\psi_0 = \begin{cases} A_{0,1}\xi_{-;1}e^{ik_{x;1}x} + A_{0,2}\xi_{-;2}e^{ik_{x;2}x}, & x \leqslant 0, \\ A_{0,3}\xi_{-;3}e^{ik_{x;3}x} + A_{0,4}\xi_{-;4}e^{ik_{x;4}x}, & x > 0. \end{cases} \tag{4}$$

The transporting dynamic for time $t > 0$ is governed by the time-dependent Schrödinger equation

$$i\frac{\partial\psi(x,t)}{\partial t} = H(x,t)\psi(x,t). \tag{5}$$

Note that here the Hamiltonian is time dependent, and it will be convenient to deal with the problem in a frame comoving with the potential. So we take the following transformation,

$$x \to x - vt, \quad t \to t, \tag{6}$$

and

$$\psi \to \psi e^{-ivx} e^{iv^2 t/2}. \tag{7}$$

Under this transformation, Eq. (5) becomes

$$i\frac{\partial \psi(x,t)}{\partial t} = H_t \psi(x,t), \tag{8}$$

with the transformed Hamiltonian being [51]

$$H_t = \frac{1}{2}\begin{bmatrix} (k_x - k_c)^2 - \Delta & \Omega \\ \Omega & (k_x + k_c)^2 + \Delta \end{bmatrix} + V_0(x), \tag{9}$$

where

$$\Delta = 2k_c v \tag{10}$$

is an effective detuning induced by the moving of the external potential.

This new time-independent Hamiltonian is similar to the Hamiltonian at time $t = 0$, except for the moving-induced additional detuning term. Therefore, the moving δ-potential also supports bound states, and these bound states can also be constructed similarly using the oscillating evanescent waves (for detail, also see Sec. III)

$$\psi_{tb} = \begin{cases} A_{t,1}\xi_{-;t1}e^{ik_{xt1}x} + A_{t,2}\xi_{-;t2}e^{ik_{xt2}x}, & x \leqslant 0, \\ A_{t,3}\xi_{-;t3}e^{ik_{xt3}x} + A_{t,4}\xi_{-;t4}e^{ik_{xt4}x}, & x > 0. \end{cases} \tag{11}$$

These states are bounded by, and at the same time, comove with the external potential and thus can serve as the transporting channels of the system. In the next section, we show that the moving δ-potential well can at most support two bound states. We label them as $\psi_{tb;g}$ and $\psi_{tb;e}$, with subscripts "g" and "e" meaning the ground and excited states. Moreover, the excited state disappears for large potential moving velocity. Hamiltonian (9) also supports an infinite number of scattering states. However, after a long-time evolution, these states spread all over the whole space and have negligible densities. Therefore, they are not important for the transportation. Neglecting them, the efficiently transported matter wave can be described by the following wave function [68,69]

$$\psi_t = C_g \psi_{tb;g} e^{-iE_g t} + C_e \psi_{tb;e} e^{-iE_e t}, \tag{12}$$

where E_g and E_e are the ground state and excited state eigenenergies, and C_g and C_e are the ground-state and excited-state probability amplitudes determined by the initial wave function according to formulas

$$C_{g,e} = \int_{-\infty}^{\infty} \psi_{tb;g,e}^{\dagger} \psi_0 e^{ivx} dx. \tag{13}$$

Here, when the excited state does not exist, one simply sets $C_e = 0$ to eliminate its role.

At last, we define some quantities to characterize the transporting efficiency of the moving δ-potential well. The time-averaged spin-$\uparrow$ and spin-$\downarrow$ atom numbers of the transported matter wave are given by

$$N_{t;\uparrow,\downarrow} = \sum_{i=g,e} \int |C_i \psi_{tb;i\uparrow,\downarrow}|^2 dx, \tag{14}$$

and the time-averaged total atom number of the transported matter wave is

$$N_t = N_{t;\uparrow} + N_{t;\downarrow} = |C_g|^2 + |C_e|^2. \tag{15}$$

We emphasize that the total atom number of the initial state ψ_0 is normalized to 1 in this paper; therefore, $N_{t;\uparrow\downarrow}$ and N_t defined here indeed can be interpreted as the fraction of transported atoms compared to the initial state.

III. TRANSPORTING CHANNELS: BOUND STATES OF THE MOVING δ-POTENTIAL WELL

From the previous section, one sees that both the initial state and the transporting channel problems involve finding the bound eigenstates of SO-coupled cold atomic matter waves. For a δ-potential well $V_0(x) = -V_0\delta(x)$, it is equivalent to a free-space problem except for the very point $x = 0$. So the bound eigenstates of a δ-potential well can be constructed using the free-particle modes by matching boundary conditions at $x = 0$ [70,71]. In this section, we first discuss the free-particle spectrum and eigenstates of a SO-coupled system, and then we construct the bound states using the free-particle modes.

The free-particle modes can be found by diagonalizing Hamiltonian (9) (with $V_0(x)$ neglected). It comes out that the eigenenergy is given by

$$\left[E - \frac{(k_x^2 + k_c^2)}{2}\right]^2 - \left(k_c k_x + \frac{\Delta}{2}\right)^2 + \left(\frac{\Omega}{2}\right)^2 = 0, \tag{16}$$

which is a second-order equation of E. This indicates that the spectrum will split into two branches (we recognize them as "lower" and "upper" branch in this paper),

$$E_{\pm} = \frac{k_x^2 + k_c^2}{2} \pm \frac{1}{2}\sqrt{(2k_c k_x + \Delta)^2 + \Omega^2}, \tag{17}$$

and the corresponding eigenstates are

$$\psi_{\pm}(k_x) = \xi_{\pm}(k_x) e^{ik_x x} = C_{\pm}\begin{pmatrix} \zeta_{\pm} \\ 1 \end{pmatrix} e^{ik_x x}, \tag{18}$$

where $\zeta_{\pm} = -(2k_c k_x + \Delta)/\Omega \pm \sqrt{(2k_c k_x + \Delta)^2/\Omega^2 + 1}$ characterize the spin wave function, and $C_{\pm} = 1/\sqrt{1 + |\zeta_{\pm}|^2}$ are the normalization parameters.

Equation (16) admits three kinds of wave vectors with real, pure imaginary, and complex value, respectively. The real part of the wave vector k_x contributes a traveling plane wave factor in the eigenstate (18), while the imaginary value part contributes an exponential decay factor. Thus, corresponding to these three kinds of wave vectors, the eigenstates are traveling plane wave, ordinary evanescent wave, and oscillating evanescent wave states, respectively [72,73]. For different strengths of SO coupling k_c and Rabi coupling Ω, the spectrum of the system can be a little different. Here we focus on the strong SO-coupling case with $k_c > \Omega/2$, and numerically we choose $k_c = 1$ and $\Omega = 0.2$ all over the paper. In Fig. 2, the free-particle spectra are plotted for different detunings $\Delta = 0$ and ± 0.1. In the figure, different types of eigenstates are marked with different styles of lines. From the figure, one sees that for energy below the minimum of the lower branch spectrum $E_0 < E_{-,\min}$, the four eigenmodes are all oscillating evanescent waves. Further calculations show that the corresponding wave vectors, i.e., solutions of Eq. (16), have the following symmetric form:

$$k_{x;1,3} = \beta \mp i\alpha_{\mathrm{I}}, \quad k_{x;2,4} = -\beta \mp i\alpha_{\mathrm{II}}. \tag{19}$$

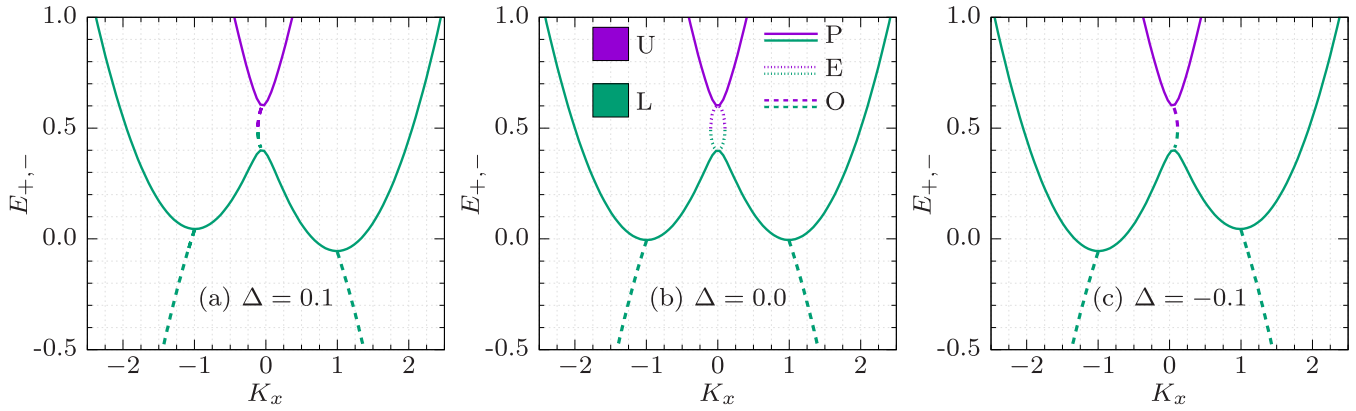

FIG. 2. Free-particle spectrum of SO-coupled cold atomic matter wave. SO-coupling and Rabi-coupling strengths are $k_c = 1$ and $\Omega = 0.2$, respectively. (a) Positive detuning $\Delta = 0.1$. (b) Zero detuning $\Delta = 0$. (c) Negative detuning $\Delta = -0.1$. The violet lines correspond to the upper (U) spectrum branch E_+, while the green lines correspond to the lower (L) spectrum branch E_-. The solid, dashed, and dotted lines represent traveling plane (P), oscillating evanescent (O), and ordinary evanescent (E) waves, respectively. For the traveling plane wave, the wave vector k_x has a real number value, and the x axis is set to $K_x = k_x$; for the oscillating evanescent wave, $k_x = \beta \pm i\alpha$, and the x axis is set to $K_x = \mathrm{sgn}[\mathrm{Re}(k_x)] \cdot |k_x|$ (therefore, the lines for $+\alpha$ and $-\alpha$ overlap with each other); and for the ordinary evanescent wave, $k_x = \pm i\alpha$, and the x axis is set to $K_x = \mathrm{sgn}[\mathrm{Im}(k_x)] \cdot |k_x|$.

Here $\alpha_{\mathrm{I,II}}$ and β are real positive numbers. Specially, when $\Delta = 0$, the two imaginary part numbers also equal each other $\alpha_{\mathrm{I}} = \alpha_{\mathrm{II}} = \alpha$.

Since waves $\exp[ik_{x;1,2}] = \exp[\pm i\beta x + \alpha_{\mathrm{I,II}} x]$ decay to zero when $x \to -\infty$, while waves $\exp[ik_{x;3,4}] = \exp[\pm i\beta x - \alpha_{\mathrm{I,II}} x]$ decay to zero when $x \to +\infty$, the bound states of a δ-potential well can be constructed using these four oscillating evanescent wave modes. The wave function can be written as

$$\psi_b = \begin{cases} A_1\xi_{-;1}e^{ik_{x;1}x} + A_2\xi_{-;2}e^{ik_{x;2}x}, & x < 0, \\ A_3\xi_{-;3}e^{ik_{x;3}x} + A_4\xi_{-;4}e^{ik_{x;4}x}, & x > 0, \end{cases}$$
$$= \begin{cases} A_1\xi_{-;1}e^{i\beta x + \alpha_{\mathrm{I}} x} + A_2\xi_{-;2}e^{-i\beta x + \alpha_{\mathrm{II}} x}, & x < 0, \\ A_3\xi_{-;3}e^{i\beta x - \alpha_{\mathrm{I}} x} + A_4\xi_{-;4}e^{-i\beta x - \alpha_{\mathrm{II}} x}, & x > 0, \end{cases} \quad (20)$$

with symbols $\xi_{-;1,2,3,4} = \xi_-(k_{x;1,2,3,4})$ for shorthand. The wave-function parameters $A_{1,2,3,4}$ and the eigenenergy E_b [$k_{x;1,2,3,4}$ are determined by E_b according to Eq. (16)] are to be determined by the normalization constraint $\int_{-\infty}^{\infty} |\psi_b|^2 dx = 1$ together with the following boundary conditions: Continuity of wave function,

$$\psi_b(x)|_{0+} = \psi_b(x)|_{0-}, \quad (21)$$

and jump of the first-order derivative of the wave function caused by the singularity of the δ-potential,

$$\left.\frac{d\psi_b(x)}{dx}\right|_{0+} - \left.\frac{d\psi_b(x)}{dx}\right|_{0-} = -2V_0\psi_b(x=0). \quad (22)$$

Because of the spin-1/2 nature of the system, a δ-potential well can support two bound states (which are recognized as ground and excited states in this paper) with spin symmetry $|\psi_\downarrow|^2 = |\psi_\uparrow|^2$ when the detuning is absent ($\Delta = 0$). When a small detuning is introduced, this spin symmetry is broken, $|\psi_\downarrow|^2 \neq |\psi_\uparrow|^2$. According to Hamiltonian (1), a positive detuning will raise the energy of the spin-$\downarrow$ (or in other words, negative momentum) component and, at the same time, lower the energy of the spin-$\uparrow$ (negative momentum) component. This fact can also be seen from the spectrum shown in Fig. 2. As a result, the ground state becomes spin-$\uparrow$ favored, while the excited state becomes spin-$\downarrow$ favored. When the detuning becomes large, the energy of the excited state will be raised out of the binding ability of the potential well, hence the excited state will disappear. For a negative detuning, the roles of spin-$\uparrow$ and spin-$\downarrow$ exchange with each other. These facts are shown in Fig. 3, where ground and excited bound states are plotted for zero and small detunings, $\Delta = 0$ and 0.1. And for large detunings, $\Delta = \pm 0.8$, the excited state disappears, and only the ground state is plotted.

We also studied the δ-potential well bounded SO-coupled spectrum. The ground-state and excited-state energies are plotted as a function of the detuning Δ in Fig. 4. The detuning induced energy splitting of the two states, and the disappearing of the excited state can be clearly seen in this figure. One can also see that for a deeper potential well the excited state disappears at a larger value of the detuning Δ. This is further shown in Fig. 5, where the excited-state disappearing critical detuning Δ_c is plotted as a function of the δ-potential well depth V_0. In this figure, in the region below the critical-value line (the black solid line), both the ground and the excited states exist, while above the line the excited state disappears, and there is only one bound state, the ground state.

At last, recalling that moving can induce an effective detuning $\Delta = 2k_c v$, it is concluded that a small positive (negative) velocity moving δ-potential well can support both a spin-$\uparrow$ (spin-$\downarrow$) favored ground-state transporting channel and a spin-$\downarrow$ (spin-$\uparrow$) favored excited-state transporting channel, while a large positive (negative) velocity moving δ-potential well can only support a spin-$\uparrow$ (spin-$\downarrow$) dominant ground-state transporting channel. This will lead to very different transporting properties of the δ-potential wells moving with different velocities.

IV. TRANSPORTATION

When the δ-potential well moves at a small velocity (moving-induced detuning fulfills $|\Delta| = 2k_c|v| < |\Delta_c|$, with

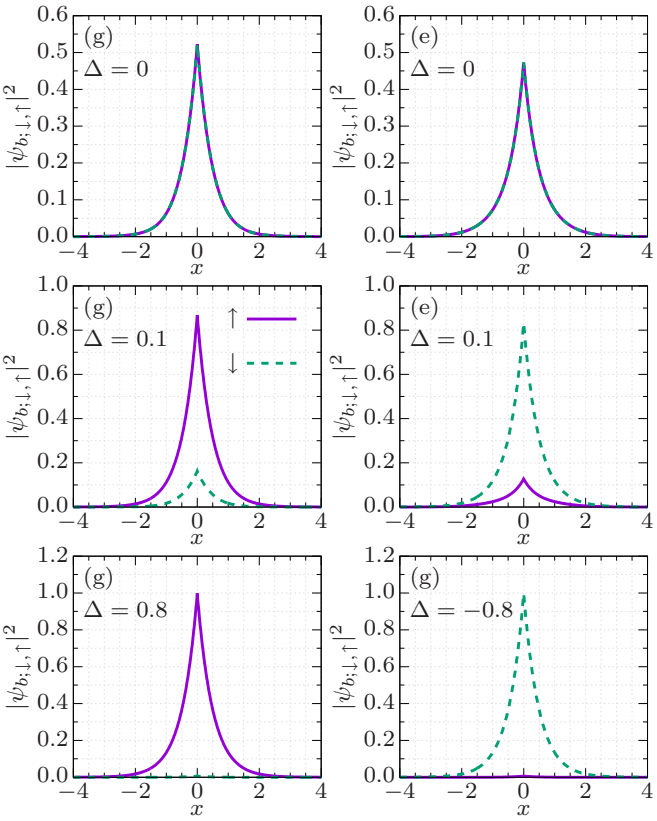

FIG. 3. Eigenstates of a δ-potential well trapped SO-coupled cold atomic matter wave for different effective detunings ($\Delta = 2k_c v = 0$, 0.1, and ± 0.8). The solid violet lines stand for the spin-$\uparrow$ component atomic density $|\psi_{b;\uparrow}|^2$, while the green dashed lines stand for the spin-$\downarrow$ component atomic density $|\psi_{b;\uparrow}|^2$. Top panels: Spin symmetric ground (g) and excited (e) states for zero detuning $\Delta = 0$. Middle panels: Spin asymmetric ground and excited states for a small detuning $\Delta = 0.1$. Bottom panels: Spin asymmetric ground states for large positive $\Delta = 0.8$ and negative detuning $\Delta = -0.8$. The excited state is absent for such large detunings, thus only the ground state is plotted. The eigenenergies corresponding to these states are -0.5536, -0.4540, -0.5742, -0.4334, -0.9056, and -0.9056, respectively. The SO-coupling and Rabi-coupling strengths are $k_c = 1$ and $\Omega = 0.2$, respectively, and the depth of the δ-potential well is $V_0 = 1$.

the critical detuning $|\Delta_c|$ having been shown in Fig. 5), both the ground-state and the excited-state channels participate in the transporting, and interference will happen between them. As a result, an oscillation of the atomic density can be observed during the transporting process. The oscillating period is determined by the energy difference between the ground and excited states, $T = 2\pi/(E_e - E_g)$. In the left panels of Fig. 6, such an oscillation is shown for a δ-potential well with depth $V_0 = 1.0$ moving at velocity $v = 0.05$. The ground-state and excited-state energies are -0.5742 and -0.4334, respectively. Therefore, the oscillating period is $T \approx 44.63$ in the figure.

When the δ-potential well moves at a large velocity ($|\Delta| = 2k_c|v| > |\Delta_c|$), the moving-induced detuning eliminates the excited-state transporting channel, and the ground-state channel plays the only transporting role. Without the excited-state

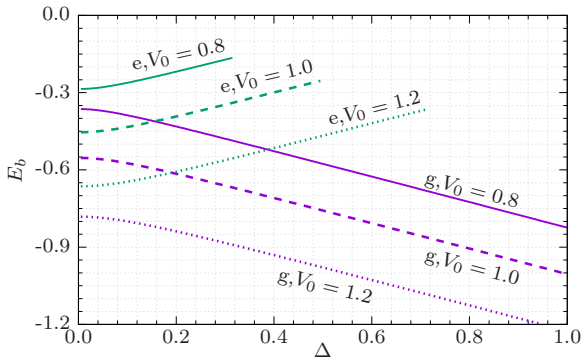

FIG. 4. The spectrum of a δ-potential bounded SO-coupled cold atomic matter wave. Ground-state (g, violet lines) and excited-state (e, green lines) energies $E_{b;g,e}$ are plotted as a function of the effective detuning $\Delta = 2k_c v$. Solid, dashed, and dotted lines represent different potential well depths $V_0 = 0.8$, 1.0, and 1.2, respectively. The SO-coupling strength and the Rabi frequency are $k_c = 1$ and $\Omega = 0.2$, respectively.

channel to interfere with, no oscillation happens in this case. For a positive-direction moving potential, the ground-state channel is spin-$\uparrow$ dominant, thus only the spin-$\uparrow$ component matter wave can be efficiently transported. While for a negative-direction moving potential, the spin-$\downarrow$ dominant ground-state channel can only efficiently transport the spin-$\downarrow$ component matter wave. This is shown in the middle and right panels in Fig. 6.

We also examined the relationship between the transporting efficiency and the moving velocity of the δ-potential well. The total transported atom number N_t and the atom number of each spin component $N_{t;\uparrow,\downarrow}$ are plotted as a function of the potential moving velocity v in Fig. 7. In the figure, below the critical velocity ($|v| < 0.25$), for a positive-direction moving potential, the spin-$\uparrow$ component is a little favored; while for a negative-direction moving potential, it is the spin-$\downarrow$ component that is favored. And the total transported atom

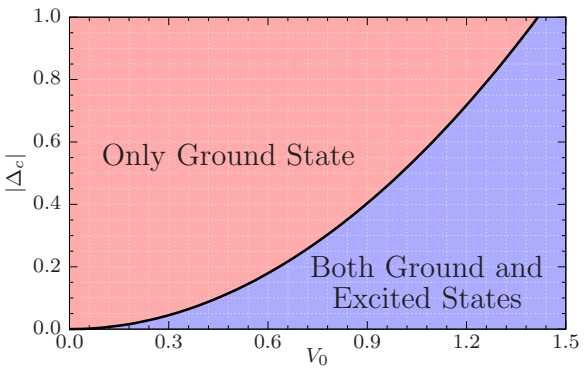

FIG. 5. Critical detuning for the disappearing of the excited state. The absolute value of critical detuning is plotted as a function of the δ-potential well depth V_0, the black solid line. Below this line, the light blue region supports both a ground and an excited bound state. While above this line, the pink region supports only one bound state, the ground state. The SO-coupling strength and the Rabi frequency are $k_c = 1$ and $\Omega = 0.2$, respectively.

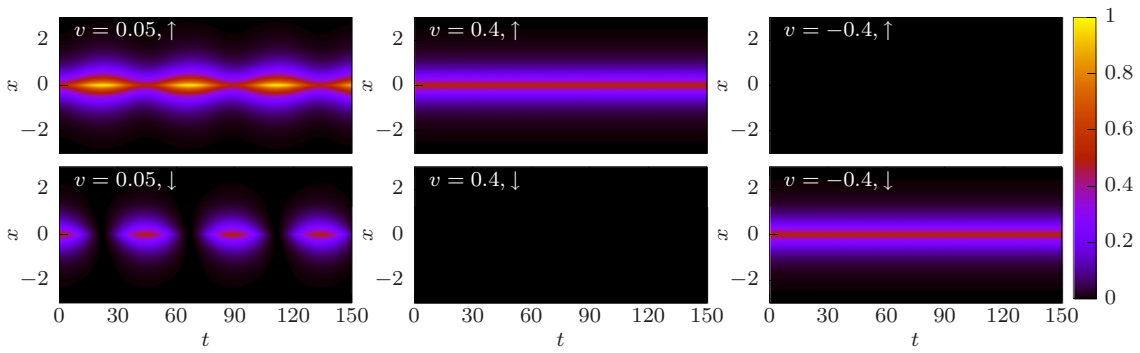

FIG. 6. Time evolution of the transported matter wave under different potential moving velocities. Left panels: Interference pattern between the ground-state and excited-state channels' transported matter wave for a small velocity ($v = 0.05$) moving δ-potential well. Middle panels: Spin-$\uparrow$ component dominant transporting for a large velocity positive-direction moving ($v = 0.4$) δ-potential well. Right panels: Spin-$\downarrow$ component dominant transporting for a large velocity negative-direction moving ($v = -0.4$) δ-potential well. The SO-coupling strength, the Rabi frequency, and the depth of the δ-potential well are $k_c = 1$, $\Omega = 0.2$, and $V_0 = 1.0$, respectively, for all plots.

number takes a value of nearly 1 (not less than 95%), which means that almost all the atoms can be transported in this case. However, when the velocity of the potential well exceeds the critical value ($|v| > 0.25$), one of the spin components (spin-$\downarrow$ for positive-direction transporting, while spin-$\uparrow$ for negative-direction transporting) suddenly drops to almost 0, and only the other spin component can still be transported. Except for this sudden dropping of transporting efficiency, in the figure one also notices a slow dropping of the total transported atom number as the transporting velocity increases. Mathematically, this is because, for a large value of v, the factor e^{ivx} in Eq. (13) contributes a fast oscillation, which will reduce the transported matter-wave amplitude. Physically, this can be explained by the fact that a faster moving of the potential tends to excite more atoms out of the trapping well.

At last, we also point out that here the moving of the δ potential is switched on abruptly. However, one can also discuss the case of adiabatically switching on. In such a case, according to the adiabatical theorem [74], the atoms will adiabatically follow the ground state of the moving potential (we assume the atoms are initially prepared in the ground state). And as we have already demonstrated the dependence of ground-state spin polarization on potential moving velocity in Sec. III, therefore the unidirectional spin transport can be achieved as well.

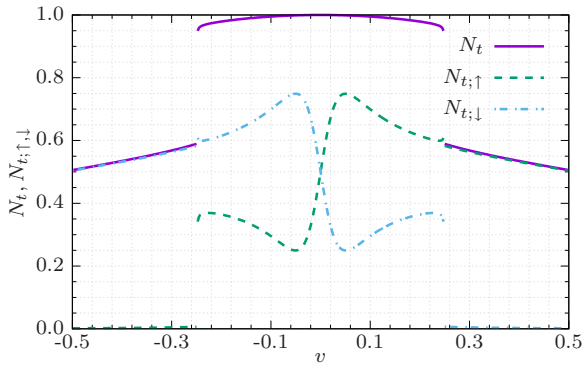

FIG. 7. Amount of transported atomic matter wave for different transporting velocities. The violet solid line represents the total amount of transported matter wave N_t defined in Eq. (15). The green dashed and cyan dash-dotted lines represent the amount of spin-$\uparrow$ and spin-$\downarrow$ components, $N_{t;\uparrow}$ and $N_{t;\downarrow}$, defined in Eq. (14). An abrupt dropping of the amount of transported matter wave happens around $v \approx \pm 0.25$, which is the critical velocity for the disappearing of the excited-state transporting channel. The parameters used are $k_c = 1.0$, $\Omega = 0.2$, and $V_0 = 1.0$.

V. SUMMARY

In summary, we have studied the transport of a SO-coupled cold atomic matter wave using a moving Dirac δ-potential well. The transporting can happen in two different channels (the ground and excited bound states of the moving δ-potential well). Because SO coupling breaks Galilean invariance, the transport shows a prominent unidirectional property. For small moving velocity, both the ground-state and the excited-state channels contribute to the transportation, and the two spin components can both be efficiently transported, where spin-$\uparrow$ (spin-$\downarrow$) is a little favored for a positive-direction (negative-direction) transport. And in such a case, the interference between the ground-state and the excited-state channels will cause an oscillation of the transported matter-wave density. When the moving velocity exceeds a critical value, the excited-state transporting channel disappears, and only one spin component of the matter wave can be efficiently transported through the ground-state channel. A positive-direction moving δ-potential well only efficiently transports the spin-$\uparrow$ component, while a negative-direction moving potential well only efficiently transports the spin-$\downarrow$ component. The critical moving velocity is also identified in the paper. Note that while some experimentally realizable potentials [64,65,75,76] can be modeled by the δ function, the phenomena reported here are expected to be observed experimentally.

ACKNOWLEDGMENTS

This work is supported by the National Natural Science Foundation of China (Grants No. 11904063, No. 11847059, and No. 11374003).

[1] T. L. Gustavson, A. P. Chikkatur, A. E. Leanhardt, A. Görlitz, S. Gupta, D. E. Pritchard, and W. Ketterle, Transport of Bose-Einstein Condensates with Optical Tweezers, Phys. Rev. Lett. **88**, 020401 (2001).

[2] M. Greiner, I. Bloch, T. W. Hänsch, and T. Esslinger, Magnetic transport of trapped cold atoms over a large distance, Phys. Rev. A **63**, 031401 (2001).

[3] J. Goldwin, S. Inouye, M. L. Olsen, B. Newman, B. D. DePaola, and D. S. Jin, Measurement of the interaction strength in a Bose-Fermi mixture with Rb87 and K40, Phys. Rev. A **70**, 021601 (2004).

[4] J. A. Sauer, K. M. Fortier, M. S. Chang, C. D. Hamley, and M. S. Chapman, Cavity QED with optically transported atoms, Phys. Rev. A **69**, 051804 (2004).

[5] F. Brennecke, T. Donner, S. Ritter, T. Bourdel, M. Köhl, and T. Esslinger, Cavity QED with a Bose-Einstein condensate, Nature (London) **450**, 268 (2007).

[6] Y. Colombe, T. Steinmetz, G. Dubois, F. Linke, D. Hunger, and J. Reichel, Strong atom-field coupling for Bose-Einstein condensates in an optical cavity on a chip, Nature (London) **450**, 272 (2007).

[7] R. Culver, A. Lampis, B. Megyeri, K. Pahwa, L. Mudarikwa, M. Holynski, P. W. Courteille, and J. Goldwin, Collective strong coupling of cold potassium atoms in a ring cavity, New J. Phys. **18**, 113043 (2016).

[8] Y. Jiang, Y. Mei, Y. Zou, Y. Zuo, and S. Du, Efficiently loading cold atomic ensemble into an optical cavity with high optical depth, in *Conference on Lasers and Electro-Optics* (OSA, Washington, DC, 2019), p. JTu2A.122.

[9] W. Bowden, R. Hobson, I. R. Hill, A. Vianello, M. Schioppo, A. Silva, H. S. Margolis, P. E. G. Baird, and P. Gill, A pyramid MOT with integrated optical cavities as a cold atom platform for an optical lattice clock, Sci. Rep. **9**, 11704 (2019).

[10] M. Bajcsy, S. Hofferberth, V. Balic, T. Peyronel, M. Hafezi, A. S. Zibrov, V. Vuletic, and M. D. Lukin, Efficient All-Optical Switching Using Slow Light within a Hollow Fiber, Phys. Rev. Lett. **102**, 203902 (2009).

[11] S. Vorrath, S. A. Möller, P. Windpassinger, K. Bongs, and K. Sengstock, Efficient guiding of cold atoms through a photonic band gap fiber, New J. Phys. **12**, 123015 (2010).

[12] M. Bajcsy, S. Hofferberth, T. Peyronel, V. Balic, Q. Liang, A. S. Zibrov, V. Vuletic, and M. D. Lukin, Laser-cooled atoms inside a hollow-core photonic-crystal fiber, Phys. Rev. A **83**, 063830 (2011).

[13] A. P. Hilton, C. Perrella, F. Benabid, B. M. Sparkes, A. N. Luiten, and P. S. Light, High-Efficiency Cold-Atom Transport Into a Waveguide Trap, Phys. Rev. Appl. **10**, 044034 (2018).

[14] T. Yoon and M. Bajcsy, Laser-cooled cesium atoms confined with a magic-wavelength dipole trap inside a hollow-core photonic-bandgap fiber, Phys. Rev. A **99**, 023415 (2019).

[15] H. Ritsch, P. Domokos, F. Brennecke, and T. Esslinger, Cold atoms in cavity-generated dynamical optical potentials, Rev. Mod. Phys. **85**, 553 (2013).

[16] L. Zhou, K. Zhang, G. Dong, and W. Zhang, Cavity quantum optics with Bose-Einstein condensates, in *Annual Review of Cold Atoms and Molecules* (World Scientific, Singapore, 2013), pp. 377–414.

[17] M. Adnan, Experimental platform towards in-fibre atom optics and laser cooling, Ph.D. thesis, Université de Limoges, 2017.

[18] M. Arndt, A. Ekers, W. von Klitzing, and H. Ulbricht, Focus on modern frontiers of matter wave optics and interferometry, New J. Phys. **14**, 125006 (2012).

[19] S. Eckel, F. Jendrzejewski, A. Kumar, C. J. Lobb, and G. K. Campbell, Interferometric Measurement of the Current-Phase Relationship of a Superfluid Weak Link, Phys. Rev. X **4**, 031052 (2014).

[20] M. Xin, W. S. Leong, Z. Chen, and S.-Y. Lan, An atom interferometer inside a hollow-core photonic crystal fiber, Sci. Adv. **4**, e1701723 (2018).

[21] C. Ryu, P. W. Blackburn, A. A. Blinova, and M. G. Boshier, Experimental Realization of Josephson Junctions for an Atom SQUID, Phys. Rev. Lett. **111**, 205301 (2013).

[22] C. Ryu and M. G. Boshier, Integrated coherent matter wave circuits, New J. Phys. **17**, 092002 (2015).

[23] A. Li, S. Eckel, B. Eller, K. E. Warren, C. W. Clark, and M. Edwards, Superfluid transport dynamics in a capacitive atomtronic circuit, Phys. Rev. A **94**, 023626 (2016).

[24] L. Amico, G. Birkl, M. Boshier, and L.-C. Kwek, Focus on atomtronics-enabled quantum technologies, New J. Phys. **19**, 020201 (2017).

[25] A. P. Chikkatur, Y. Shin, A. E. Leanhardt, D. Kielpinski, E. Tsikata, T. L. Gustavson, D. E. Pritchard, and W. Ketterle, A continuous source of Bose-Einstein condensed atoms, Science **296**, 2193 (2002).

[26] T. Lahaye, G. Reinaudi, Z. Wang, A. Couvert, and D. Guéry-Odelin, Transport of atom packets in a train of Ioffe-Pritchard traps, Phys. Rev. A **74**, 033622 (2006).

[27] W. Guerin, J.-F. Riou, J. P. Gaebler, V. Josse, P. Bouyer, and A. Aspect, Guided Quasicontinuous Atom Laser, Phys. Rev. Lett. **97**, 200402 (2006).

[28] M. Kasevich, D. S. Weiss, E. Riis, K. Moler, S. Kasapi, and S. Chu, Atomic Velocity Selection Using Stimulated Raman Transitions, Phys. Rev. Lett. **66**, 2297 (1991).

[29] K. Gibble and S. Chu, Laser-Cooled Cs Frequency Standard and a Measurement of the Frequency Shift Due to Ultracold Collisions, Phys. Rev. Lett. **70**, 1771 (1993).

[30] M. J. Renn, D. Montgomery, O. Vdovin, D. Z. Anderson, C. E. Wieman, and E. A. Cornell, Laser-Guided Atoms in Hollow-Core Optical Fibers, Phys. Rev. Lett. **75**, 3253 (1995).

[31] H. Ito, T. Nakata, K. Sakaki, M. Ohtsu, K. I. Lee, and W. Jhe, Laser Spectroscopy of Atoms Guided by Evanescent Waves in Micron-Sized Hollow Optical Fibers, Phys. Rev. Lett. **76**, 4500 (1996).

[32] D. Müller, D. Z. Anderson, R. J. Grow, P. D. D. Schwindt, and E. A. Cornell, Guiding Neutral Atoms Around Curves with Lithographically Patterned Current-Carrying Wires, Phys. Rev. Lett. **83**, 5194 (1999).

[33] J. Denschlag, D. Cassettari, and J. Schmiedmayer, Guiding Neutral Atoms with a Wire, Phys. Rev. Lett. **82**, 2014 (1999).

[34] M. Key, I. G. Hughes, W. Rooijakkers, B. E. Sauer, E. A. Hinds, D. J. Richardson, and P. G. Kazansky, Propagation of Cold Atoms Along a Miniature Magnetic Guide, Phys. Rev. Lett. **84**, 1371 (2000).

[35] K. E. Strecker, G. B. Partridge, A. G. Truscott, and R. G. Hulet, Formation and propagation of matter-wave soliton trains, Nature (London) **417**, 150 (2002).

[36] A. E. Leanhardt, A. P. Chikkatur, D. Kielpinski, Y. Shin, T. L. Gustavson, W. Ketterle, and D. E. Pritchard, Propagation of

Bose-Einstein Condensates in a Magnetic Waveguide, Phys. Rev. Lett. **89**, 040401 (2002).
[37] L. Plaja and L. Santos, Expansion of a Bose-Einstein condensate in an atomic waveguide, Phys. Rev. A **65**, 035602 (2002).
[38] S. Gupta, K. W. Murch, K. L. Moore, T. P. Purdy, and D. M. Stamper-Kurn, Bose-Einstein Condensation in a Circular Waveguide, Phys. Rev. Lett. **95**, 143201 (2005).
[39] J. Bravo-Abad, M. Ibanescu, J. D. Joannopoulos, and M. Soljačić, Photonic crystal optical waveguides for on-chip Bose-Einstein condensates, Phys. Rev. A **74**, 053619 (2006).
[40] A. L. Marchant, T. P. Billam, T. P. Wiles, M. M. H. Yu, S. A. Gardiner, and S. L. Cornish, Controlled formation and reflection of a bright solitary matter-wave, Nat. Commun. **4**, 1865 (2013).
[41] W. Hänsel, J. Reichel, P. Hommelhoff, and T. W. Hänsch, Magnetic Conveyor Belt for Transporting and Merging Trapped Atom Clouds, Phys. Rev. Lett. **86**, 608 (2001).
[42] S. Schmid, G. Thalhammer, K. Winkler, F. Lang, and J. H. Denschlag, Long distance transport of ultracold atoms using a 1D optical lattice, New J. Phys. **8**, 159 (2006).
[43] A. Couvert, T. Kawalec, G. Reinaudi, and D. Guéry-Odelin, Optimal transport of ultracold atoms in the non-adiabatic regime, Europhys. Lett. **83**, 13001 (2008).
[44] A. Alberti, V. V. Ivanov, G. M. Tino, and G. Ferrari, Engineering the quantum transport of atomic wavefunctions over macroscopic distances, Nat. Phys. **5**, 547 (2009).
[45] R. Roy, P. C. Condylis, V. Prakash, D. Sahagun, and B. Hessmo, A minimalistic and optimized conveyor belt for neutral atoms, Sci. Rep. **7**, 13660 (2017).
[46] K. O. Chong, J.-R. Kim, J. Kim, S. Yoon, S. Kang, and K. An, Observation of a non-equilibrium steady state of cold atoms in a moving optical lattice, Commun. Phys. **1**, 25 (2018).
[47] K. Zhou and Z. Zhang, Opposite Effect of Spin-Orbit Coupling on Condensation and Superfluidity, Phys. Rev. Lett. **108**, 025301 (2012).
[48] J. P. Vyasanakere and V. B. Shenoy, Collective excitations, emergent Galilean invariance, and boson-boson interactions across the BCS-BEC crossover induced by a synthetic Rashba spin-orbit coupling, Phys. Rev. A **86**, 053617 (2012).
[49] Y. Zhang, M. E. Mossman, T. Busch, P. Engels, and C. Zhang, Properties of spin-orbit-coupled Bose-Einstein condensates, Front. Phys. **11**, 118103 (2016).
[50] Q. Zhu, C. Zhang, and B. Wu, Exotic superfluidity in spin-orbit coupled Bose-Einstein condensates, Europhys. Lett. **100**, 50003 (2012).
[51] J.-Y. Zhang, S.-C. Ji, Z. Chen, L. Zhang, Z.-D. Du, B. Yan, G.-S. Pan, B. Zhao, Y.-J. Deng, H. Zhai, S. Chen, and J.-W. Pan, Collective Dipole Oscillations of a Spin-Orbit Coupled Bose-Einstein Condensate, Phys. Rev. Lett. **109**, 115301 (2012).
[52] Y. Li, G. I. Martone, and S. Stringari, Sum rules, dipole oscillation and spin polarizability of a spin-orbit coupled quantum gas, Europhys. Lett. **99**, 56008 (2012).
[53] Y. Xu, Y. Zhang, and B. Wu, Bright solitons in spin-orbit-coupled Bose-Einstein condensates, Phys. Rev. A **87**, 013614 (2013).
[54] C. Hamner, Y. Zhang, M. A. Khamehchi, M. J. Davis, and P. Engels, Spin-Orbit-Coupled Bose-Einstein Condensates in a One-Dimensional Optical Lattice, Phys. Rev. Lett. **114**, 070401 (2015).
[55] Y.-C. Zhang, Z.-Q. Yu, T. K. Ng, S. Zhang, L. Pitaevskii, and S. Stringari, Superfluid density of a spin-orbit-coupled Bose gas, Phys. Rev. A **94**, 033635 (2016).
[56] M. E. Mossman, J. Hou, X.-W. Luo, C. Zhang, and P. Engels, Experimental realization of a non-magnetic one-way spin switch, Nat. Commun. **10**, 3381 (2019).
[57] C.-H. Li, C. Qu, R. J. Niffenegger, S.-J. Wang, M. He, D. B. Blasing, A. J. Olson, C. H. Greene, Y. Lyanda-Geller, Q. Zhou, C. Zhang, and Y. P. Chen, Spin current generation and relaxation in a quenched spin-orbit-coupled Bose-Einstein condensate, Nat. Commun. **10**, 375 (2019).
[58] L. W. Cheuk, A. T. Sommer, Z. Hadzibabic, T. Yefsah, W. S. Bakr, and M. W. Zwierlein, Spin-Injection Spectroscopy of a Spin-Orbit Coupled Fermi Gas, Phys. Rev. Lett. **109**, 095302 (2012).
[59] J. Lan, W. Yu, R. Wu, and J. Xiao, Spin-Wave Diode, Phys. Rev. X **5**, 041049 (2015).
[60] Y.-J. Zhao, D. Yu, L. Zhuang, X. Gao, and W.-M. Liu, Tunable spinful matter wave valve, Sci. Rep. **9**, 8653 (2019).
[61] M. Lebrat, S. Häusler, P. Fabritius, D. Husmann, L. Corman, and T. Esslinger, Quantized Conductance through a Spin-Selective Atomic Point Contact, Phys. Rev. Lett. **123**, 193605 (2019).
[62] L. Corman, P. Fabritius, S. Häusler, J. Mohan, L. H. Dogra, D. Husmann, M. Lebrat, and T. Esslinger, Quantized conductance through a dissipative atomic point contact, Phys. Rev. A **100**, 053605 (2019).
[63] Y.-J. Lin, K. Jimenez-Garcia, and I. B. Spielman, Spin-orbit-coupled Bose-Einstein condensates, Nature (London) **471**, 83 (2011).
[64] H. Uncu, D. Tarhan, E. Demiralp, and Ö. E. Müstecaplıoğlu, Bose-Einstein condensate in a harmonic trap decorated with Dirac δ functions, Phys. Rev. A **76**, 013618 (2007).
[65] M. C. Garrett, A. Ratnapala, E. D. van Ooijen, C. J. Vale, K. Weegink, S. K. Schnelle, O. Vainio, N. R. Heckenberg, H. Rubinsztein-Dunlop, and M. J. Davis, Growth dynamics of a Bose-Einstein condensate in a dimple trap without cooling, Phys. Rev. A **83**, 013630 (2011).
[66] C. Chin, R. Grimm, P. Julienne, and E. Tiesinga, Feshbach resonances in ultracold gases, Rev. Mod. Phys. **82**, 1225 (2010).
[67] E. Timmermans, P. Tommasini, M. Hussein, and A. Kerman, Feshbach resonances in atomic Bose-Einstein condensates, Phys. Rep. **315**, 199 (1999).
[68] E. Granot and A. Marchewka, Quantum particle displacement by a moving localized potential trap, Europhys. Lett. **86**, 20007 (2009).
[69] E. Sonkin, B. A. Malomed, E. Granot, and A. Marchewka, Trapping of quantum particles and light beams by switchable potential wells, Phys. Rev. A **82**, 033419 (2010).
[70] J. Qin, R. Zheng, and L. Zhou, Bound states of spin-orbit coupled cold atoms in a Dirac delta-function potential, J. Phys. B: At., Mol. Opt. Phys. **53**, 125301 (2020).
[71] L. Rossi, F. Dolcini, and F. Rossi, Majorana-like localized spin density without bound states in topologically trivial spin-orbit coupled nanowires, Phys. Rev. B **101**, 195421 (2020).
[72] V. A. Sablikov and Y. Y. Tkach, Evanescent states in two-dimensional electron systems with spin-orbit interaction and

spin-dependent transmission through a barrier, Phys. Rev. B **76**, 245321 (2007).

[73] L. Zhou, J.-L. Qin, Z. Lan, G. Dong, and W. Zhang, Goos-Hänchen shifts in spin-orbit-coupled cold atoms, Phys. Rev. A **91**, 031603(R) (2015).

[74] T. Kato, On the adiabatic theorem of quantum mechanics, J. Phys. Soc. Jpn. **5**, 435 (1950).

[75] M. Łacki, M. A. Baranov, H. Pichler, and P. Zoller, Nanoscale "Dark State" Optical Potentials for Cold Atoms, Phys. Rev. Lett. **117**, 233001 (2016).

[76] Y. Wang, S. Subhankar, P. Bienias, M. Łacki, T.-C. Tsui, M. A. Baranov, A. V. Gorshkov, P. Zoller, J. V. Porto, and S. L. Rolston, Dark State Optical Lattice with a Subwavelength Spatial Structure, Phys. Rev. Lett. **120**, 083601 (2018).